Silicon RF-Photonic Filter and Down-Converter

Silicon RF-Photonic Filter and Down-Converter

Kun-Yii Tu, Mahmoud S. Rasras, Douglas M. Gill, Sanjay S. Patel, Young-Kai Chen, *Fellow, IEEE*, Alice E. White, *Member, IEEE*, Andrew Pomerene, Daniel Carothers, James Beattie, Mark Beals, Jurgen Michel, and Lionel C. Kimerling

***Abstract*—An RF-photonic filter and down-converter system based on a compact and fully tunable silicon optical filter has been demonstrated and analyzed. Its frequency down-conversion was implemented using optical heterodyne detection with an injection locked laser. This system filters a 1.25 GHz-wide signal with $>$ 20 dB filter rejection and a very broad 20 GHz center tuning range. The frequency down-conversion process is operated in a low-IF mode to avoid laser low frequency noises. Measured system Spurious-Free Dynamic Range (SFDR) of 94.3 dB*Hz$^{2/3}$ has been limited by the optical losses from I/O coupling and measurement setup. We examined experimentally that 105.3 dB*Hz$^{2/3}$ SFDR is achievable if the encountered optical loss were reduced to the filter's intrinsic loss. Based on the excellent agreements between measured and simulated results, we explore the critical improvements of the silicon photonic devices needed for the system to achieve 118 dB*Hz$^{2/3}$ SFDR and briefly review the status of the component technologies.**

***Index Terms*—Coherent detection, microwave-photonic filter, RF-photonic filter, silicon photonics, ultra wide band filter.**

I. Introduction

MILITARY industries continue to have strong interest in ultra-wide-bandwidth RF-photonic systems, primarily due to their ability to deliver performance with unprecedented high time-bandwidth product [1]. As communication/electronic warfare systems evolve to handle applications involving commercial cellular, fixed wireless, and high frequency radars all in a single platform, the system instantaneous bandwidth might reach 100 GHz. Designing with a conventional approach for such high spectral range would yield a complex system with enormous size, weight and power consumption. Though the speed of modern semiconductor devices already supports RF IC with bandwidths exceeding many tens of gigahertz, there is still not a filter technology competitive enough to facilitate radio operations with a similar bandwidth. Recent tunable filters (mostly MEMS or LTCC cavity-based) have center frequencies that are confined to a range of less than 10 GHz [2]–[4] and, due to a limited quality factor (Q), are expected to have relative bandwidths of 0.5–6%. Since much higher Q can be achieved with RF-photonic techniques, RF-photonic filters can be tuned over a wider range and with much less bandwidth variation, making them attractive options for operations up to 100 GHz operating range.

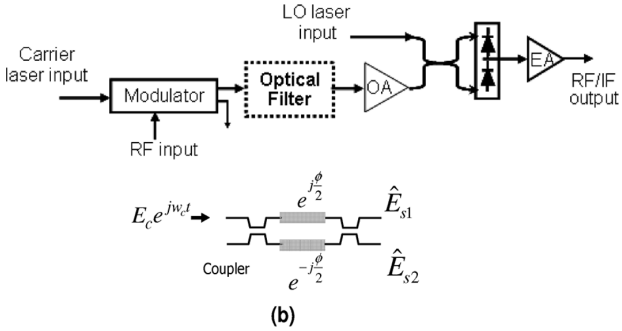

Fig. 1. (a) Block diagram of RF-Photonic filter implemented with coherent detection. OA stands for optical amplifier and EA electrical amplifier (b) Model of MZ modulator.

Traditionally, RF-photonic filters were implemented with optical fiber Bragg gratings, fiber Fabry–Perot filters, or array waveguide gratings [5]. Designing a large system such as a broadband channelizer [6] with these traditional filters, the growth of physical size and complexity involved for accurate frequency tuning becomes a concern. To that extent, compact photonic filters based on a highly integrated platform [7]–[9] would be favorable. Recent silicon CMOS photonic ring-based filters have been shown with a Q factor on the order of 200 000 [7], owing to greatly reduced photonic waveguide losses [10]. Because of silicon's high index contrast waveguides, a higher density of integration can be achieved to construct scalable systems with minimal component mismatch. Given that CMOS photonics technologies have been successfully demonstrated with optical detectors and modulators integrated on-chip [11], an entire complex signal processor on a single monolithic CMOS platform may be feasible in the near future.

To demonstrate the power of CMOS-based RF-photonics, we constructed a complete system using a CMOS tunable optical bandpass filters reported in 2007 by Rasras *et al.* [7]. Each filter, with an area of 3.5 mm $\times$ 0.25 mm, exhibits an adjustable optical bandwidth of $<$800 MHz tunable over a 20 GHz frequency range [7]. The same filter was also reconfigured to form a microwave notch filter [12] to illustrate its functional flexibility. By implementing the frequency down-conversion process with an optical heterodyne technique, our RF-photonic filter and down-converter can be used to enable a 1.25 GHz-wide RF signal processing with 20 dB stop-band rejection and 20 GHz tuning range. Overall, an in-band system

Manuscript received March 04, 2010; revised June 14, 2010; accepted July 12, 2010. Date of publication September 02, 2010; date of current version October 06, 2010. This work was supported by the Defense Advanced Research Projects Agency under its EPIC program. The program was executed by the Microsystems Technology Office (MTO) with Dr. Jagdeep Shah's supervision under Contract No. HR0011-05-C-0027.

K.-Y. Tu, M. S. Rasras, D. M. Gill, S. S. Patel, Y.-K. Chen and A. E. White are with Alcatel-Lucent Technologies, Bell-Labs., Murray Hill, NJ 07974 USA (phone: 908-582-5566; e-mail: kun-yii.tu@alcatel-lucent.com).

A. Pomerene, D. Carothers and J. Beattie are with BAE Systems, Nashua, NH 03061 USA (e-mail: james.beattie@baesystems.com).

M. Beals, J. Michel, and L. C. Kimerling are with Massachusetts Institute of Technology, Massachusetts 02139 USA (e-mail: lckim@MIT.EDU).

Color versions of one or more of the figures in this paper are available online at http://ieeexplore.ieee.org.

Digital Object Identifier 10.1109/JLT.2010.2072952

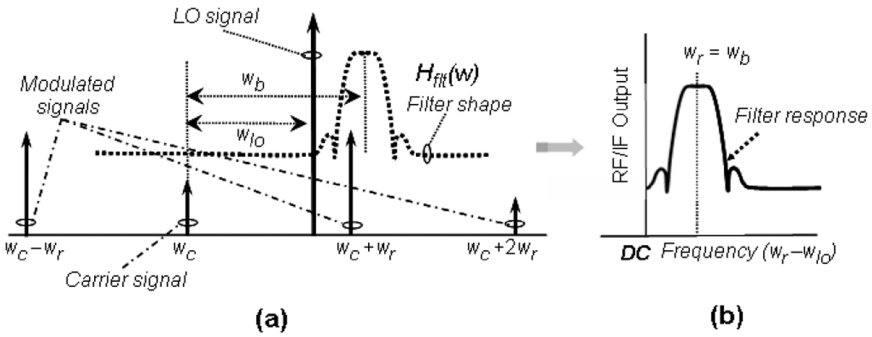

Fig. 2. (a) Drawing showing spectral relationship between the optical bandpass filter response, the modulated signals and the LO signal. (b) The spectrum of the bandpass filter measured at RF/IF output.

gain of 1 dB and SFDR of 94.3 dB*Hz$^{2/3}$ was achieved. The SFDR was severely limited by the optical losses from filter I/O coupling, polarization mismatches, and other imperfections in our experimental setup. To understand the impact of these optical losses, we replaced the optical filter with an attenuation equivalent to the filter's intrinsic loss and achieved an SFDR of 105.3 dB*Hz$^{2/3}$. The latter, though an approximation, helps to estimate the improvement from minimizing I/O losses through system integration. For both experiments, our comprehensive analysis achieved very good agreement with measured results.

This paper presents the first demonstration of an RF-photonic bandpass filter and down-converter system based on a CMOS optical filter. This design can be used as a starting point for building more complex systems with high bandwidth performance. Because the silicon photonics field is still relatively new, further improvements will be necessary to achieve a high end SFDR. We investigate the performance of future components required for meeting new challenges and review several recent component breakthroughs.

II. RF-Photonic Filter and Down-Converter System

In general, RF-photonic filters can be implemented with either direct or coherent detection techniques. For the former, a broadband RF signal can be optically modulated, filtered, and converted back to an RF signal directly by an optical receiver (the diagram of a coherent detection system shown in Fig. 1(a) can be modified to show a direct detection system by bypassing the photonic local oscillator (LO) laser and the coupler). Such an approach may be straightforward but requires broadband detectors and amplifiers, since the filtered narrowband signals can still have a very high center frequency. Because ADC performance degrades when its spectral coverage increases, the signal at the detector would have to be converted to baseband with an RF mixer before digital sampling in order to achieve high system dynamic range. As the system complexity grows, it can become costly and power hungry since many high speed circuits are required. The excessive heat generated by these circuits can create problems for managing the temperature-sensitive photonic components.

Coherent detection systems, on the other hand, provide the ability to down-convert high frequency RF input to a low-intermediate frequency (IF) output by beating the optically filtered signal with the photonic LO signal. As illustrated in Fig. 1(a), a very broad band RF signal at frequency w_r is up-converted to optical frequency ($w_c + w_r$ or $w_c - w_r$) by an optical modulator, where w_r extends over the modulator's bandwidth and w_c is a fixed carrier laser frequency. This up-converted signal is then filtered by a tunable CMOS optical filter, and subsequently mixed with the LO at $w_c + w_{\rm lo}$ at the coupler and balanced detector. This generates the down-converted signal at the IF frequency $w_r - w_{\rm lo}$. The spectral relevance between signals can be better visualized with Fig. 2(a), where the optical filter response is overlaid with the modulator output signals and the LO. In this example, the filter center frequency is tuned to $w_c + w_b$ to capture the positive sideband of the modulated signal at $w_c + w_r$, where w_b is the center frequency of the desired RF signal. Since the filter is tuned to the positive side of w_c, the lower sideband signal at $w_c - w_r$ and the carrier at w_c would be reduced at the filter stop band.

Typically, the system output frequency response (Fig. 2(b)) can be characterized by measuring the output spectrum while sweeping the RF input frequency (w_r) with fixed w_c, w_b and $w_{\rm lo}$. As part of the system frequency plan, given a band of desirable RF input signal, the center frequency of the output signal $(w_b - w_{\rm lo})$ should be adjusted to minimize unwanted spurious. As an example, it is convenient and beneficial to move the filter passband away from the LO frequency to suppress the noises caused by the LO low frequency spurious. Moreover, by lowering the IF frequency, the bandwidth of the detectors and amplifiers can be greatly reduced, as well as the amplifier/system power consumption. Details of the filter operation will be further clarified in the following system analysis.

III. System Analysis

Besides the filter's spectral response, important performance metrics of RF-photonic systems include Gain, Noise Figure (NF) and Linearity (IP3). In general, SFDR summarizes these system metrics, but in some cases NF may be explicitly required.

A. System Gain

For our analysis, a modulator model is assumed, as indicated in Fig. 1(b), where a Mach–Zehnder Intensity modulator (MZI) was made by an interferometer formed with two phase shifters. These phase shifters generate opposite phase shifts $\phi(t)/2$ and $-\phi(t)/2$ according to differential voltage inputs with a common factor:

$$\phi(t) = \frac{\pi}{V_\pi}[V_{\rm DC} + \nu(t)] \tag{1}$$

where $\nu(t)$ represents a small RF signal superposed on a DC biased voltage $V_{\rm DC}$. V_π is the DC voltage required for a modulator phase shift of π radians. Assuming a single tone RF input, $\nu(t) = \nu_r \sin w_r t$, the optical field $\hat{E}_{s1}$ at the MZI output becomes

$$\hat{E}_{s1} = jE_c \sin\left[\frac{\pi}{2V_\pi}(V_{\rm DC} + \nu_r \sin w_r t)\right] \bullet e^{jw_c t}. \tag{2}$$

The magnitude of E_c can be derived from the master laser power $(P_{c,\rm in})$ by $|E_c| = \sqrt{P_{c,\rm in}L_{c1}}$ where L_{c1} includes the master laser output splitter loss and the modulator insertion loss. For a small signal $|\nu(t)| \le 1$, we expand the optical field $\hat{E}_{f1}$ at the filter output and retain the relevant frequency components at w_c, $w_c + w_r$, and $w_c - w_r$ as shown below

$$\begin{aligned}\hat{E}_{f1} &= \hat{E}_{s1} * h_{\rm flt}(t)\\ &\cong \left[\hat{E_{s1}}\Big|_{V=V_{\rm DC}} + \frac{\partial \hat{E}_{s1}}{\partial \nu}\Big|_{V=V_{\rm DC}} \nu(t)\right] * h_{\rm flt}(t)\\ &\cong jE_c \sin\left(\frac{\Gamma_0}{2}\right) H_{\rm flt}(w_c) e^{jw_c t}\\ &\quad + \left(\frac{E_c \pi v_r}{4V_\pi}\right) \cos\left(\frac{\Gamma_0}{2}\right) H_{\rm flt}(w_c + w_r) e^{j(w_c + w_r)t}\\ &\quad - \left(\frac{E_c \pi v_r}{4V_\pi}\right) \cos\left(\frac{\Gamma_0}{2}\right) H_{\rm flt}(w_c - w_r) e^{j(w_c - w_r)t}\end{aligned} \tag{3}$$

where $h_{\rm flt}(t)$ and $H_{\rm flt}(w)$ represent the filter's time domain impulse response and frequency response, respectively, and * denotes a convolution operator. Details on the $H_{\rm flt}(w)$ of our CMOS optical filter can be found in [7]. According to (3), because of the MZI modulator, detailed signal and carrier conditioning can be accomplished by varying DC phase $\Gamma_0 = \pi V_{\rm DC}/V_\pi$. Note that, for simplicity, the input and output coupling losses (I/O losses) of the optical filter and the loss due to polarization mismatch are also included in these filter responses, represented by $H_{\rm flt}(w_c)$, $H_{\rm flt}(w_c + w_r)$ and $H_{\rm flt}(w_c - w_r)$.

Because the filter is single-ended, we can only construct a partially balanced system (Fig. 1), which applies single-ended modulation but balanced detection. To derive the in-band system gain, we retain from (3) only the frequency component at $w_c + w_r$, since the other two are significantly attenuated by the optical filter. For implementations involving loss from coupling signals in and out of a filter chip, an optical amplifier with power gain $(G_{\rm oa})$ may be needed for compensation. In that respect, the signal field should be scaled accordingly.

Before beating the signal with the LO, we first describe the actual received photonic LO by

$$\hat{E}_{\rm lo} = E_{\rm lo} e^{j(w_c + w_{\rm lo})t} \tag{4}$$

where the field magnitude $|E_{\rm lo}|$ relates to its source power $P_{\rm lo,in}$ by $|E_{\rm lo}| = \sqrt{P_{\rm lo,in}L_{c2}}$ with L_{c2} accounting for the insertion loss of the coupler. By coupling the two optical fields, $\hat{E}_{\rm lo}$ and $\hat{E}_{f1}(w_c + w_r)$, and beating them at the balanced detector, we obtained two electrical currents

$$I_{d1} = [I_{f1} + I_{\rm lo} + I_{\rm sig}\sin((w_r - w_{\rm lo})t + \Delta\phi)]/2 \tag{5}$$

and

$$I_{d2} = [I_{f1} + I_{\rm lo} - I_{\rm sig}\sin((w_r - w_{\rm lo})t + \Delta\phi)]/2 \tag{6}$$

For simplicity, $\Delta\phi$ sums up the DC phase terms between the optical fields and the filter response. I_{f1}, $I_{\rm lo}$ and $I_{\rm sig}$ can be further expressed by

$$\begin{aligned}I_{f1} &= RP_{c,\rm in}L_{c1}G_{\rm oa}L_{c2}\\ &\quad \times |H_{\rm flt}(w_c + w_r)|^2 \left(\frac{\pi\nu_r}{2V_\pi}\right)^2 \cos^2\left(\frac{\Gamma_0}{2}\right)\end{aligned} \tag{7}$$

$$I_{\rm lo} = RP_{lo,\rm in}L_{c2} \tag{8}$$

$$\begin{aligned}I_{\rm sig} &= R\sqrt{P_{c,\rm in}L_{c1}G_{\rm oa}L_{c2}P_{lo,\rm in}L_{c2}}\\ &\quad \times |H_{\rm flt}(w_c + w_r)| \left(\frac{\pi\nu_r}{2V_\pi}\right) \cos\left(\frac{\Gamma_0}{2}\right).\end{aligned} \tag{9}$$

where R represents the responsivity of the detectors. I_{f1} and $I_{\rm lo}$ represent the DC currents resulting from the self-beating of the modulated signal and LO. Even though their currents are cancelled at the balanced detector output, it is important to keep I_{f1} and $I_{\rm lo}$ because their shot noise contributions still add up. From (5) and (6), the AC current $(I_{\rm out})$ is calculated by taking the difference between I_{d1} and I_{d2}, where

$$\begin{aligned}I_{\rm out} &= R\sqrt{P_{c,\rm in}L_{c1}G_{\rm oa}L_{c2}P_{lo,\rm in}L_{c2}}|H_{\rm flt}(w_c + w_r)|\\ &\quad \bullet \left(\frac{\pi\nu_r}{2V_\pi}\right) \cos\left(\frac{\Gamma_0}{2}\right) \sin[(w_r - w_{\rm lo})t + \Delta\phi].\end{aligned} \tag{10}$$

Based on $I_{\rm out}$ and the matching impedances (Z_0) of the detector and modulator, the system RF gain can be evaluated by

$$\begin{aligned}G_{\rm RF} &= \frac{\text{RF output power}}{\text{RF input power}}\\ &= P_{c,\rm in}L_{c1}G_{\rm oa}L_{c2}P_{\rm lo,in}L_{c2}\\ &\quad \times \left[R\pi Z_0 |H_{\rm flt}(w_c + w_r)| \cos\left(\frac{\Gamma_0}{2}\right)/4V_\pi\right]^2\end{aligned} \tag{11}$$

where $Z_0 = 50\ \Omega$. A few things worth noting are: 1) due to the detector matching there was an extra 6 dB power loss, which could be avoided if the detectors were integrated closely with an electronic amplifier; 2) in this case, the system gain can clearly be maximized at $\Gamma_0 = 2n\pi, n = 0, 1, 2\ldots$, rather than at the quadrature point commonly used in direct detection systems; 3) the RF filter attenuation scales dB-per-dB with the optical filter's power attenuation; 4) a factor of two less in modulator efficiency comes from using the single-ended modulator output.

B. Noise Figure

The noise output of this coherent heterodyne system with an OA on its signal path can be summarized in the following:

$$N_{\rm total} = N_{\rm noncan} + \gamma \times N_{\rm can} \tag{12}$$

where $N_{\rm noncan}$ represents the noise terms that are not cancellable from balanced detection and $N_{\rm can}$ represents those cancellable ones. Here, γ accounts for the effectiveness of the

noise cancellation from balance detection, i.e., $\gamma = 0$ means a full cancellation.

Balanced detection in a coherent detection system cannot cancel the RIN- and ASE-induced noises involving cross beating between a RIN/ASE noise from one path and the signals from its opposite path [13]. Evidently, shot and thermal noise are also not cancellable. In detail, $N_{\rm noncan}$ is given by

$$N_{\rm noncan} = \frac{4kT_0}{Z_0}\left(\frac{G_{\rm RF}}{2}+1\right) + 2q(I_{\rm lo}+I_{f1}) + 4I_{\rm lo}RS_{\rm ase} + 2I_{\rm lo}I_{f1}\sqrt{t_{\rm lorin}t_{\rm sigrin}} + 4qRS_{\rm ase}B_{\rm oa} \quad (13)$$

where the individual terms represent contributions from, respectively: 1) thermal noise from the modulator and detector matching impedances, 2) shot noise from the LO and signal, 3) beat noise between the LO itself and the ASE noise from the signal path, 4) beat noise between the LO RIN and the signal RIN, and 5) shot noise due to ASE. The ASE noise from OA can be quantified with $S_{\rm ase} = n_{\rm sp}(G_{\rm oa}-1)hf$, where $n_{\rm sp} = (10^{\xi/10})/2, h =$ Planck's constant, $f =$ the optical frequency, and $\xi =$ OA's noise figure in dB. $t_{\rm lorin}$ and $t_{\rm sigrin}$ represent the RIN factors associated with LO and signal lasers, and, without additional noise filtering, $B_{\rm oa}$ is simply the optical bandwidth of the OA. Note that the thermal noise given by the first term of (13) is similar to that of the direct detection system [14], except the contribution from the modulator matching has been reduced because of the optical filtering. The shot noise given by the second term of (13) is dominated by the LO signal $(I_{\rm lo})$. However, it is the third term of (13) that typically dominates the output noise in systems implemented with high LO power and OA gain to combat high optical loss. Since the OA is placed after the filter, its ASE noise bandwidth is much higher than the signal bandwidth, so an extra factor of 2 must be considered in the noise term. Both polarizations have been considered for those ASE self-induced noise.

On the contrary, the cancellable noises from balanced detection involve the beating between RIN/ASE noises with the signal or LO from the same source path and can be expressed by

$$N_{\rm can} = I_{f1}^2 t_{\rm sigrin} + I_{\rm lo}^2 t_{\rm lorin} + 4I_{f1}RS_{\rm ase} + 4R^2S_{\rm ase}^2B_{\rm oa} \quad (14)$$

where the individual terms represent contributions from, respectively: 1&2) RIN noises from signal and LO paths, 3) beat noise between ASE noise and the signal, 4) ASE-ASE beat noise.

Using (11) and (12), we can represent the final system noise figure as

$$\mathrm{NF} = \frac{N_{\rm total}Z_0}{4kTG_{\rm RF}}. \quad (15)$$

Based on (3) and (11), using an MZI modulator allows the system gain to be maximized while reducing the optical carrier and its associated noise. Such a benefit may not be available if using a different type of modulator. In general, although the RIN and ASE associated noise cancellation presented here cannot be as complete as that of a balanced direct detection system, at least the major RIN noise from the LO self beating can still be reduced by balancing the 2×2 coupler and the detectors. For those interested, some of the relevant noise discussions may also be found in [13]–[17].

C. Distortion (Linearity)

To obtain the in-band input IP3, we examine the modulator output signal $(\hat{E}_{s1})$ directly and leave out the filter and detectors. Since the third order inter-modulation product (IMD3) is created only at the modulator, if we referred to the system input, IP3 should not be affected by the filter or detectors (assuming the detectors handle high optical power and are linear). As discussed before, from (3), (5) and (6), the RF signal at the detector is proportional to the modulator output optical field and not its power, so the IP3 can be derived based on $\hat{E}_{s1}$ alone from (1) and (2), with the RF input replaced by a two-tone signal $\nu(t) = \nu_{r1}\sin w_{r1}t + \nu_{r2}\sin w_{r2}t$. Therefore, IMD3 should appear at the optical frequencies $2w_{r1}-w_{r2}+w_c$ and $2w_{r2}-w_{r1}+w_c$, which are down-converted to IF frequencies at $(2w_{r1}-w_{r2})-w_{\rm lo}$ and $(2w_{r2}-w_{r1})-w_{\rm lo}$ after beating with the LO at the detectors. By expanding $\hat{E}_{s1}$ in a polynomial form based on small signal approximations and equating the first order and third order frequency components, the input IP3 voltage can be obtained by

$$\nu_{r1,\rm IIP3} = \left[8\left.\frac{\partial\hat{E}_{s1}}{\partial\nu_1}\right|_{V=V_{\rm DC}} \Big/ \left.\frac{\partial^3\hat{E}_{s1}}{\partial\nu_1^3}\right|_{V=V_{\rm DC}}\right]^{1/2} \quad (16)$$

which leads to simple expressions of IIP3 voltage and power

$$v_{r1,\rm IIP3} = \frac{\sqrt{32}V_\pi}{\pi} \text{ and } P_{\rm IIP3} = \frac{v_{r1,\rm IIP3}^2}{2Z_0} \quad (17)$$

Compared to a direct detection system, this IIP3 power is two times (6 dB) higher given the same magnitude of V_π [18] and is independent of the modulator DC bias (Γ_0).

D. SFDR

Applying (15) and (17), the SFDR of this coherent heterodyne detection system can be obtained with

$$\mathrm{SFDR}|_{\mathrm{dB}*\mathrm{Hz}^{2/3}} = \frac{2}{3}[P_{\rm IIP3}|_{\rm dBm} - (-174+\mathrm{NF}|_{\rm dB})]. \quad (18)$$

For a system requiring further electrical amplification, its cascaded gain, NF, and IP3 can be calculated with conventional formulations for 50 Ω matched systems (details are omitted here).

IV. Experimental Setup and Results

Homodyne techniques can also be applied for coherent detection, for example, by bypassing the MZ2 DFB laser and circulator in Fig. 3(a) and using the master laser simultaneously as both the source for photonic LO and the signal carrier. However, even though its principle is sound, we found experimentally that the RF signal can fluctuate substantially due to the beating between the signal's carrier and the LO, whose phases vary after traveling through different fibers.

On the contrary, in a heterodyne design the problem is resolved by introducing a frequency offset to the LO with an injection-locked DFB laser. As shown in Fig. 3(a), MZ2 takes a

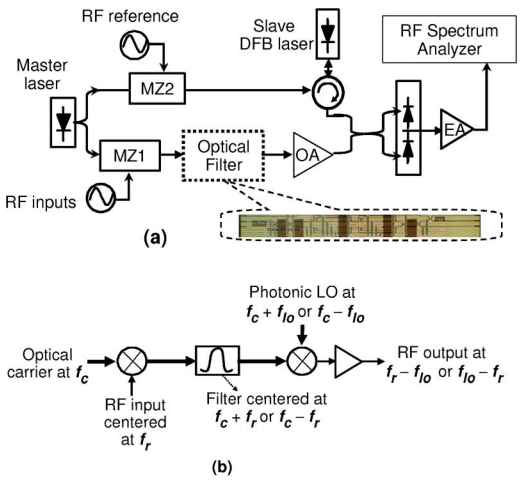

Fig. 3. (a) Detail block diagram of experimental set up with the inset showing the actual CMOS optical filter. (b) Frequency relationship between signals.

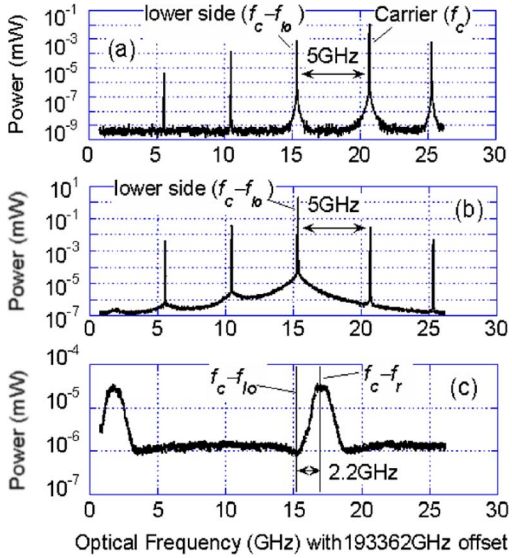

Fig. 4. (a) Optical spectrum of injection signal from MZ2 where $f_c = 193383$ GHz (1551.33 nm wavelength) and $f_{\rm lo} = 5$ GHz, (b) Optical spectrum of the injection-locked LO signal from DFB laser, injection-locking to the lower sideband of $f_c - f_{\rm lo}$, (c) Optical spectrum of the optical filter with filter center tuned to 2.2 GHz offset from the LO on the low side.

small portion of the master laser light (frequency f_c) and modulates it with an RF reference signal (frequency $f_{\rm lo}$) to generate a comb of injection source signals with strongest sidebands at $f_c - f_{\rm lo}$ (lower side) and $f_c + f_{\rm lo}$ (upper side), where $f = w/2\pi$. So, while the DFB laser is injected by these source signals from MZ2, its cavity resonance is thermally tuned to within the locking range of either the lower sideband at $f_c - f_{\rm lo}$ or the upper sideband at $f_c + f_{\rm lo}$ to reach an injection locked state. The LO signal generated is then coherent with the master laser signal (or carrier signal) with a frequency offset of $f_{\rm lo}$. The unwanted LO harmonics at multiples of $f_{\rm lo}$ away from f_c can be suppressed further with an extra optical filter if necessary. To capture a specific band of RF signal centered at f_r in an optical lower sideband operation, given an RF LO at $f_{\rm lo}$, the center of the optical filter and optical LO frequencies should be tuned to $f_c - f_r$ and $f_c - f_{\rm lo}$ respectively. In an optical upper sideband operation the negative signs become positive. After detection at the detector, the output RF frequencies would either be $f_r - f_{\rm lo}$ if $f_r > f_{\rm lo}$ (for an RF upper sideband down-conversion), or $f_{\rm lo} - f_r$ if $f_{\rm lo} > f_r$ (for an RF lower sideband down-conversion). Fig. 3(b) illustrates some of the frequency relationships between various components in the system where the first mixer symbolizes the optical modulator as an up-converter and the second mixer symbolizes the detector as a down-converter. In general, the CMOS filter was tuned thermo-electrically for bandwidth and center frequency adjustments. In terms of signal quality, since the optical filter does single-side-band filtering, better image rejection can be achieved with high stop-band rejection at the image and/or by applying a single sideband modulator.

With regards to experimental procedures, without the recently available high resolution (20 MHz) optical complex spectrum analyzer (OCSA), the alignment of the optical filter, as well as the modulated signal and the LO signal with a sub-GHz frequency precision, would pose a formidable challenge. As an example, the spectral relationship between the optical injection signal from MZ2 (Fig. 4(a)), the photonic LO signal generated from the side-band-injected DFB laser (Fig. 4(b)), and the optical spectrum of the CMOS optical filter (Fig. 4(c)) can be visualized while each frequency is tuned. Note that a 5 GHz separation between the carrier and the sidebands is chosen for the injection source (i.e., $f_{\rm lo} = 5$ GHz), and the slave DFB laser is tuned and injection-locked to the first lower sideband. In this case, 15 dB rejection of the LO's spurious rejection is given without any optical filtering. Fig. 4(c) illustrates the filter being tuned to the lower sideband of the LO (i.e., $f_r < f_{\rm lo}$) by a -2.2 GHz offset, with the filter response exhibiting a 15 GHz free spectral range. This filter spectrum was captured by injecting broadband optical noise into the filter and optically amplified afterward. Given the high noise level involved in this observation, the filter rejection is not accurately conveyed. However, this measurement was quite useful for tuning purposes.

The ultra wide frequency tuning range of our RF-photonic system is demonstrated in Fig. 5(a), (b), (c), and (d), where the down-converted RF output spectra were shown with $f_{\rm lo}$ set to 5, 8, 10, and 15 GHz, and the corresponding filters were centered at 2.25 GHz, 10 GHz, 12 GHz, and 17.5 GHz from the carrier. These plots show the RF input frequency spectrum covered from 0.5 GHz to 20 GHz, limited by the available RF synthesizer and the modulator, but not by the CMOS optical filter. All cases were based on optical lower sideband and RF upper sideband operations, except Fig. 5(a), where an RF lower sideband operation was used to specifically avoid LO beating with the carrier. In Fig. 5(a), the unwanted tone at 5 GHz caused by LO-spurious and LO-carrier mixings can be easily filtered out at the baseband. A slight tilt of the spectrum in Fig. 5(d) was observed, mainly due to higher roll-off close to the band edge of the modulator that can be equalized electronically. All filter bandwidths achieved were close to 1.25 GHz, and the stop band rejections were better than 20 dB. In fact, optical filter rejection >25 dB was observed at 1553 nm optical wavelength, but it was beyond the tuning range of our master laser. In general, fine-tuning would depend on the accuracy of the on-chip

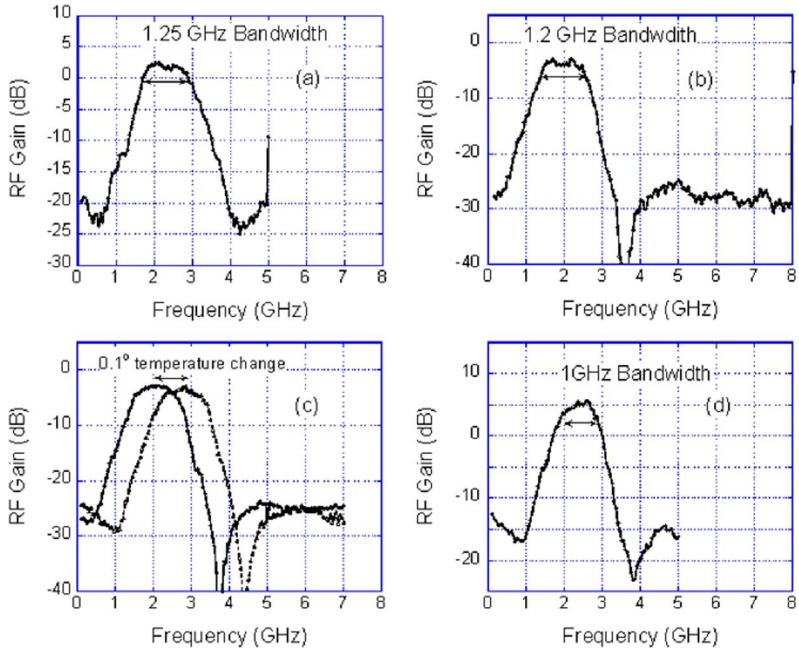

Fig. 5. (a) RF bandpass filter response with $f_{\rm lo} = 5$ GHz. Here, the signal is captured at lower sideband. 5 GHz spurious from LO-spurious beating is also shown. (b) Bandpass filtering with $f_{\rm lo} = 8$ GHz, signal on the upper side of LO. (c) Tuning of the filter with 0.1 deg of temperature change. Here, $f_{\rm lo} = 10$ GHz. (d) Bandpass with $f_{\rm lo} = 15$ GHz showing the highest band captured.

thermo-electric heaters; a 25 MHz tuning accuracy was demonstrated optically [7]. Nevertheless, coarse tuning of the filter can be easily done by temperature controlling the filter's mounting base using a thermo-electric cooler (TEC). Fig. 5(c) illustrates a coarse 1 GHz tuning of the filter center frequency with 0.1 degree TEC adjustment. In this experimental setup, the master laser puts out 84 mW power at 1551.33 nm wavelength, from which 95% goes to MZ1 for signal modulation and 5% goes to MZ2 for sideband injection. The injection-locked DFB laser outputs 2.5 mW optical power at the first lower sideband and is directly joined with the modulated and filtered signal at a 2×2 coupler. MZ1 is a 20 GHz balanced modulator with V_π of 2.1 V and 7 dB insertion loss. The characterization of the optical filter with an optical LUNA VOA indicates a 15 dB in-band optical loss, including 6 dB of intrinsic loss and 9 dB of facet losses. Unfortunately, due to the extra losses from the polarization controller and polarization mismatches between components in our optical probing system, the best in-band optical loss increases to 26.7 dB. This loss was measured by comparing the power of the modulated optical signal before and after the filter at the in-band frequency using OCSA. We expect this excessive loss to be dramatically reduced when this filter chip is integrated with other components. A 20 GHz bandwidth balanced detector at the 2×2 fiber coupler outputs were applied for optical signal detection. Two EAs with total gain of 30 dB, 4.5 dB NF, 13 GHz bandwidth, and 32.8 dBm output IP3 were applied at the detector output to increase RF system gain to a single digit level.

For RF system measurements, we operated the system in two configurations: (i) with the integrated CMOS optical filter followed by an optical amplifier (OA) to compensate the filter and other excessive losses, and (ii) with the optical filter and the OA replaced by a simple 6 dB attenuator to explore the baseline performance, assuming that the excessive I/O loss can be reduced, for example, by integrating modulators and detectors on chip. In case (i) the OA provides 23 dB gain using a 30 mA pump. We placed the OA after the filter simply to avoid chances of burning our sample, even though reversing the sequence would lower system noise. The linearity and the output noise measurement results are shown in Fig. 6(a), where measured SFDR for case (i) is 54.3 dB*MHz$^{2/3}$ or 94.3 dB*Hz $^{2/3}$ and for case (ii) is 65.3 dB*MHz $^{2/3}$ or 105.3 dB*Hz$^{2/3}$. System gain for both cases is close to 1 dB, since the OA pump current was adjusted to match the gain between case (i) and (ii). Both systems' IIP3s are about 22 dBm and the impact from the post-amplifiers is insignificant. Output noise levels for case (i) and (ii) are shown in Fig. 6(b) based on measurements from single-ended and balanced detectors. Measured gain improvements due to the balanced detector over single-ended detectors is about 5 dB, indicating slight imbalance at the coupler and detectors. As expected, only limited noise cancellation was achieved due to this rather simple setup we applied. Nevertheless, these various measurement configurations help to determine the noise cancellation factors and provide a crosscheck between results from several analyses. Good agreement between the measured and analyzed results were shown in Table I for both cases, which confirm that our analysis is comprehensive enough for further design optimization and technology assessments.

It is quite obvious that reducing system optical losses by having modulator and detectors integrated on the same chip can directly impact the system performance. However, achieving the SFDR close to 120 dB*Hz$^{2/3}$ desired for many applications [22] will require that several serious challenges are met. Fig. 7(a)–(c) illustrates the simulated performances of SFDR, NF, and Gain versus variations of V_π and laser carrier power. 50 mW of LO power was assumed based on the current achievable DFB laser power and the heat management consideration in

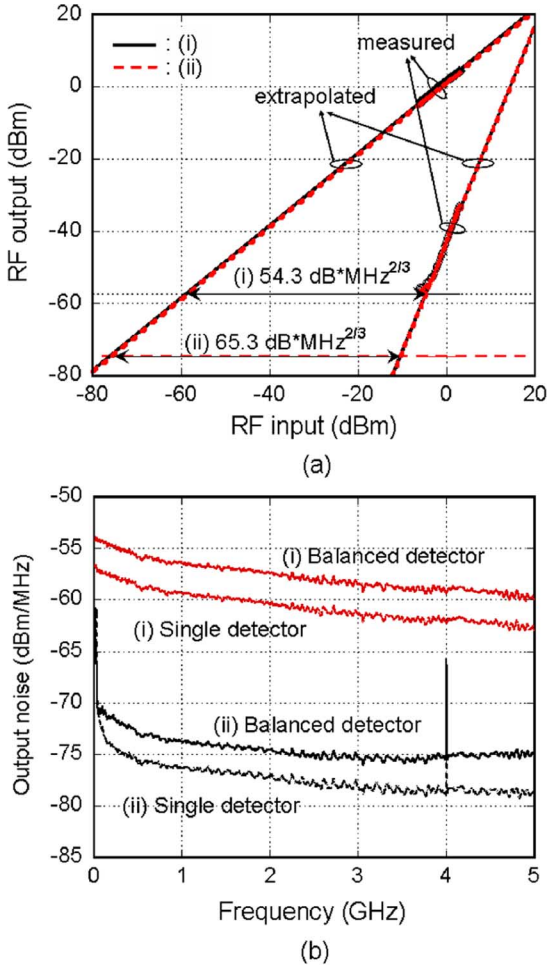

Fig. 6. (a) Measured linearity, noise and SFDR of the RF-photonic bandpass filter and down-converter. Case (i) represents system implemented with CMOS filter cascaded with an OA. Case (ii) represents filter and OA replaced with a 6 dB attenuator. In this measurement $f_{\mathrm{lo}} = 8$ GHz, RF two tones at 11.800 and 11.801 GHz were chosen to coincide with the filter center at their optically modulated frequencies. (b) Measured output noises for case (i) and (ii) with a single-ended detector and a balanced detector.

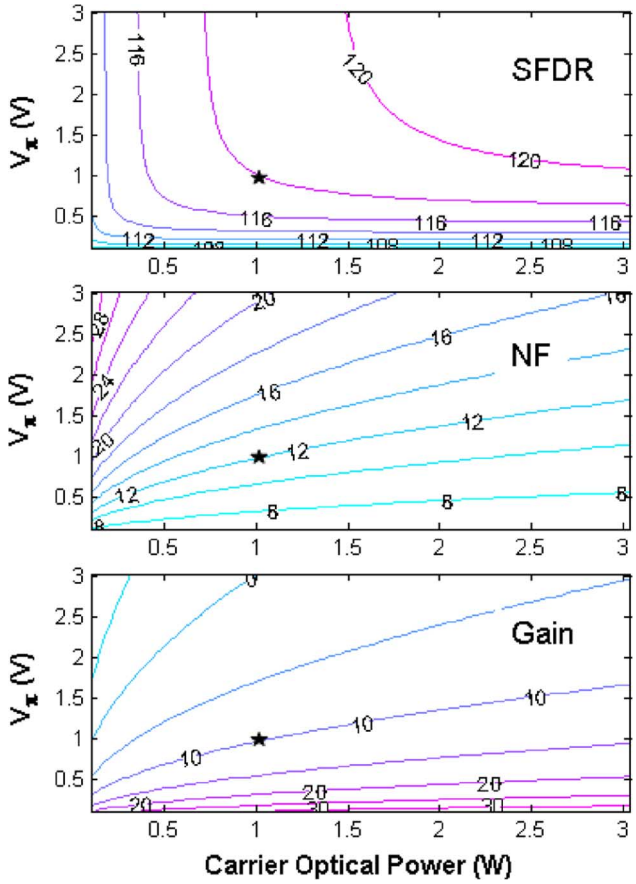

Fig. 7. (a) Simulated system SFDR, (b) NF and (c) Gain versus V_π and carrier optical power of an RF-Photonic filter and down-converter. An achievable state of 118 dB*Hz$^{2/3}$ SFDR has been marked with * signs.

a scaled up system. Since the cross beating between LO and signal RIN noise cannot be cancelled by a balanced detector, the RIN noise requirement of the carrier laser is raised to -175 dBc/Hz. The noise cancellation from balanced detection is lowered to 0.01 (-20 dB) for reducing those cancellable noises. There is no electrical and optical amplifier involved, and the 6 dB loss caused by the detector's resistive matching is eliminated. With these requirements fulfilled, an SFDR of 118 dB*Hz$^{2/3}$ can be achieved with a 1 V V_π and a 1 W carrier optical power, as indicated by * in Fig. 7. A 12 dB NF and 10 dB gain for a filter and down-converter with 15 dBm input IP3 would be considered quite competitive for many ultra broadband applications. To further improve NF, placing a single low gain and high linearity low noise electrical amplifier in front would be sufficient.

Given the size of the optical filters, it is conceivable that a sophisticated RF-photonic system can be built with a single silicon chip ($\sim$400 filters/2 $\times$ 2.5 cm reticle). However, optimal system performance will depend on the success of silicon detector and modulator integrations. To date, Ge detector and silicon modulator research has primarily focused on digital applications. Ge detectors at 1550 nm have been developed with impressive responsivity (1 A/W), bandwidth (25 GHz) [19]–[21], and dark current (<1 μA) [20], [21]. However, no specifics regarding power handling and linearity performances, which are important for analog applications, were mentioned. Silicon modulator designs [23]–[28] are beginning to achieve bandwidths comparable to those of $LiNbO_3$ modulators. The $LiNbO_3$ modulators, with $>$20 GHz bandwidth and 1 V V_π, have been shown to handle $>$1 W input power in analog links with single digit NF and 120 dB*Hz$^{2/3}$ SFDR up to 12 GHz [22]. A silicon modulator based on free carrier plasma dispersion effect was shown to reach 30 GHz bandwidth with 4 V-cm push-pull V_π L product [23]. It was reported that, in a micro-ring-assisted silicon MZI [24], bandwidth was increased to 35 GHz, together with a 25% V_π L improvement. By hybrid integration with an AlGaInAs Multi-Quantum-Well, the electro-optics effect was enhanced in a 500 μm evanescent MZI to achieve a 2 V-mm V_π L [27]. However, while high bandwidth is the focus of digital modulators with some consideration for V_π, in analog systems, low V_π and high power handling are as important as high bandwidth. Compared to the $LiNbO_3$, the V_π values of the silicon modulators are still much higher, and it is not clear that the power handling of the silicon modulators can reach 1 W without introducing serious nonlinearities. So far, power handling issues have not been addressed except in [27], which claimed a 28 mW 1 dB-compression.

TABLE I
PARAMETERS (APPLIED AND MEASURED)

Parameters	Value (case i/ii)	Unit
Source laser power	84	mW
Signal loss	–26.7/–5.4	dB
LO laser power	2.5	mW
Detector responsivity	0.65	A/W
Coupler 1 loss	0.45	dB
Coupler 2 loss	1	dB
MZI insertion loss	–7	dB
MZI V_π	2.1	V
MZI bias	$\pi/8$	V
MZI output (carrier, calculated)	-2.9	dBm
MZI output (carrier, measured)	-3.3	dBm
MZI output (signal, calculated)	-4.5	dBm
MZI output (signal, measured)	-6.2	dBm
RF input power	3	dBm
OA gain	23/0	dB
OA bandwidth	1530-1565	nm
Laser RIN	-154	dBc
Temperature	293	K
Optical wavelength	1550	nm
Modulator input load	50	Ohm
Detector load	50	Ohm
Electrical amplifier gain	30	dB
Electrical amplifier NF	3.5	dB
Electrical amplifier IP3	29.8	dBm
Noise cancellation factor	0.76/0.51	
Calculated gain	2.0/0.3	dB
Measured gain	1.7/1.2	dB
Calculated IIP3	21.0/21.5	dBm
Measured IIP3	22.2/22.1	dBm
Calculated SFDR	94.1/105.5	$dB*Hz^{2/3}$
Measured SFDR	94.5/105.3	$dB*Hz^{2/3}$

Because silicon modulators might not be of a conventional MZI type, the optical response to a driving signal is no longer a simple trigonometric function (e.g., (2)). V_π is not necessarily an accurate indicator for a modulator's linearity performance; (16)–(17) may be more appropriate for quantifying the actual IP3. In addition, some of these silicon modulators' extinction ratios drop substantially when their bandwidths go up. When a system needs good carrier suppression and a high compression point, this might become a drawback. Since bandwidth, V_π, and optical power handling are related, designing modulators for the RF-photonic applications will require a serious design trade-off between them. Optimization processes demonstrating the capability of designing a 15 GHz bandwidth and 0.886 V-cm V_π L modulator would be helpful for future success [29].

As system performance improves with better silicon photonics components, a low-RIN carrier laser becomes critical for the beat noise elimination needed for the few remaining dBs of system SFDR improvement. A recently reported Photonic Systems Inc. laser with a -172 dBc RIN level seems promising [22]. Also, with matched detectors, an accurately tuned coupler, and on-chip electronics all integrated, balanced detection can be improved without resorting to bulky discrete tuning devices. Certainly, the system complexity and functionality will always benefit from further reduction of the waveguide losses.

V. CONCLUSION

We demonstrated a complete RF-photonic filter and down-converter system based on a compact and fully tunable CMOS optical filter. This RF-photonic system filters a 1.25 GHz-wide RF signal with center frequency tunable over an ultrawide range of 20 GHz while maintaining 20 dB of stop band attenuation. The filtered signal was down-converted to a low-IF frequency by using optical heterodyne detection achieved with an injection-locked photonic LO. The measured SFDR of 94.3 $dB*Hz^{2/3}$ was primarily limited by high losses from I/O coupling and imperfections of our experimental setup. Baseline measurements indicated that a SFDR better than 105.3 $dB*Hz^{2/3}$ is achievable if filter I/O losses were eliminated through monolithic integration of modulators and detectors. Based on the good agreement we achieved between analysis and experiments, we explored the challenges ahead for silicon photonic devices and the source laser to support a system at an 118 dB*Hz SFDR level.

ACKNOWLEDGMENT

The views, opinions, and/or findings contained in this article/presentation are those of the author/presenter and should not be interpreted as representing the official views or policies, either expressed or implied, of the Defense Advanced Research Projects Agency or the Department of Defense.

Approved for Public Release, Distribution Unlimited.

REFERENCES

[1] S. A. Pappert and B. Krantz, "RF photonics for radar front-ends," in *Proc. Radar Conference*, 2007, pp. 965–970.

[2] K. Entesari and G. M. Rebeiz, "A 12–18 GHz three-pole RF MEMS tunable filter," *IEEE Trans. Microw. Theory Tech.*, vol. 53, no. 8, pp. 2566–2571, 2005.

[3] K. Entesari and G. M. Rebeiz, "A differential 4-bit 6.5–10 GHz RF MEMS tunable filter," *IEEE Trans. Microw. Theory Tech.*, vol. 53, no. 3, pp. 1103–1110, 2005.

[4] H. Joshi, H. H. Sigmarsson, D. Peroulis, and W. J. Chappell, "Highly loaded evanescent cavities for widely tunable high-Q filters," in *Proc. IEEE MTT Microwave Symp.*, 2007, pp. 2133–2136.

[5] J. Capmany, B. Ortega, and D. Pastor, "A tutorial on microwave photonic filters," *J. Lightw. Technol.*, vol. 24, no. 1, pp. 201–229, Jan. 2006.

[6] M. E. Manka, "Microwave photonics for electronic warfare applications," in *Proc. IEEE MWP'08 Conf.*, 2008, pp. 175–178.

[7] M. S. Rasras, D. M. Gill, S. S. Patel, K.-Y. Tu, Y.-K. Chen, A. E. White, A. T. Pomerene, D. N. Carothers, M. J. Grove, D. K. Sparacin, J. Michel, M. A. Beals, and L. C. Kimerling, "Demonstration of a fourth-order pole-zero optical filter integrated using CMOS processes," *J. Lightw. Technol.*, vol. 25, no. 1, pp. 87–92, Jan. 2007.

[8] Y. B. E. Little, S. T. Chu, P. P. Absil, J. V. Hryniewicz, F. G. Johnson, F. Seiferth, D. Gill, V. Van, O. King, and M. Trakalo, "Very high-order microring resonator filters for WDM applications," *IEEE Photon. Technol. Lett.*, vol. 16, no. 10, pp. 2263–2265, Oct. 2004.

[9] T. Barwicz, M. A. Popovic, M. R. Watts, P. T. Rakich, E. P. Ippen, and H. I. Smith, "Fabrication of add-drop filters based on frequency-matched microring resonators," *J. Lightw. Technol.*, vol. 24, no. 5, pp. 2207–2218, May 2006.

[10] D. K. Sparacin, S. J. Spector, and L. C. Kimerling, "Silicon waveguide sidewall smoothing by wet chemical oxidation," *J. Lightw. Technol.*, vol. 23, no. 8, pp. 2455–2461, Aug. 2005.

[11] B. Analui, D. Gukenberger, D. Kucharski, and A. Narasimha, "Fully integrated 20 Gb/s optoelectronic transceiver implemented in a standard 0.13 um CMOS SOI technology," *IEEE J. Solid-State Circuits*, vol. 41, no. 12, pp. 2945–2955, Dec. 2006.

[12] M. S. Rasras, K. Y. Tu, D. M. Gill, Y. K. Chen, A. E. White, S. S. Patel, A. Pomerene, D. Carothers, J. Beattie, M. Beals, J. Michel, and L. C. Kimerling, "Demonstration of a tunable microwave-photonic notch filter using low-loss silicon ring resonators," *J. Lightw. Technol.*, vol. 27, no. 12, pp. 2105–2110, Dec. 2005.

[13] S. Yamashita and T. Okoshi, "Suppression of beat noise from optical amplifiers using coherent receivers," *J. Lightw. Technol.*, vol. 12, no. 6, pp. 1029–1035, Jun. 1994.

[14] E. I. Ackerman, C. Cox, III, G. Betts, H. Roussell, K. Ray, and F. O'Donnell, "Input impedance conditions for minimizing the noise figure of an analog optical lLink," *IEEE Trans. Microw. Theory Tech.*, vol. 46, no. 12, pp. 2025–2031, Dec. 1998.

[15] D. M. Sabido and L. G. Kazovsky, "Dynamic range of optically amplified RF optical links," *IEEE Trans. Microw. Theory Tech.*, vol. 49, no. 10, pp. 1950–1955, Oct. 2001.

[16] S. Ryu, S. Yamamoto, H. Taga, Y. Yoshida, and H. Wakabayashi, "Long haul coherent optical fiber communication systems using optical amplifiers," *J. Lightw. Technol.*, vol. 9, no. 2, pp. 251–260, Feb. 1991.

[17] N. A. Olsson, "Lightwave systems with optical amplifiers," *J. Lightw. Technol.*, vol. 7, no. 7, pp. 1071–1082, Jul. 1989.

[18] A. S. Daryoush, E. Ackerman, N. R. Samant, S. Wanuga, and D. Kasemset, "Interfaces for high speed fiber-optics links: Analysis and experiment," *IEEE Trans. Microw. Theory Tech.*, vol. 39, no. 12, pp. 2031–2044, 1991.

[19] L. Vivien, M. Rouviere, J. Fedeli, D. Marris-Morini, J. Damlencourt, J. Mangeney, P. Crozat, L. El Mehaoui, E. Cassan, X. Le Roux, D. Pascal, and S. Laval, "High speed and high responsivity germanium photodetector integrated in a silicon-on-insulator microwaveguide," *Opt. Exp.*, vol. 15, no. 15, pp. 9843–9848, 2007.

[20] D. Ahn, C.-Y. Hong, J. Liu, M. Beals, L. C. Kimerling, J. Michel, J. Chen, and F. X. Kaertner, "High performance, waveguide integrated Ge. photo detectors," *Opt. Exp.*, vol. 15, no. 17, pp. 3916–3921, 2007.

[21] K.-W. Ang, S. Zhu, M. Yu, G.-Q. Lo, and D.-L. Kwong, "High performance waveguided Ge-on-SOI metal-semiconductor-metal photodetectors with novel silicon-carbon schottky barrier enhancement layer," *IEEE Photon. Technol. Lett.*, vol. 20, no. 9, pp. 754–756, May 2008.

[22] E. I. Ackerman, W. K. Burns, G. E. Betts, J. X. Chen, J. L. Prince, M. D. Regan, H. V. Roussell, and C. H. Cox, "RF-Over-Fiber links with very low noise figure," *J. Lightw. Technol.*, vol. 26, no. 15, pp. 2441–2448, Aug. 2008.

[23] L. Liao, A. Liu, D. Rubin, J. Basak, Y. Chetrit, H. Nguyen, R. Cohen, N. Izhaky, and M. Paniccia, "40 Gbit/s silicon optical modulator for high-speed applications," *Electron. Lett.*, vol. 43, no. 22, pp. 1196–1197, 2007.

[24] D. M. Gill, M. Rasras, K.-Y. Tu, Y. K. Chen, A. White, S. S. Patel, D. Carothers, A. Pomerere, R. Kamocsai, C. Hill, and J. Battie, "Internal bandwidth equalization in a CMOS compatible Si ring modulator," *IEEE Photon. Technol. Lett.*, vol. 21, no. 4, pp. 200–202, Feb. 2009.

[25] Q. Xu, S. Manipatruni, B. Schmidt, J. Shaya, and M. Lipson, "12.5 Gbits/s carrier injection-based silicon microring modulators," *Opt. Exp.*, vol. 15, pp. 430–436, 2007.

[26] J. Liu, D. Pan, S. Jongthammanurak, S. Wada, J. C. Kimerling, and J. michel, "Design of monolithically integrated GeSi electroabsoption modulators and photodetectors on an SOI platform," *Opt. Exp.*, vol. 15, 2007.

[27] H. W. Chen, Y. H. Kuo, and J. E. Bowers, "High speed hybrid silicon evanescent Mach–Zehnder modulator and switch," *Opt. Exp.*, vol. 16, no. 25, pp. 20571–20576, 2008.

[28] D. Marris-Morini, L. Vivien, J. M. Fedeli, E. Cassan, P. Lyan, and S. Laval, "Low loss and high speed silicon optical modulator based on a lateral carrier depletion structure," *Opt. Exp.*, vol. 16, no. 1, pp. 334–339, 2008.

[29] V. M. N. Passaro and F. Dell'Olio, "Scaling and optimization of MOS optical modulators in Nanometer SOI waveguides," *IEEE Trans. Nanotechnol.*, vol. 7, no. 4, pp. 401–408, 2008.

Kun-Yii Tu (M'03) received the B.S. degree from National Chiao-Tung University, Hsin-Chu, Taiwan, in 1979, the M.Sc. degree from Northwestern University, Evanston, IL in 1985, and the Ph.D. degree from Polytechnic Institute of New York University, New York, in 1992, all in electrical engineering.

His academic research involved high-temperature microwave applicator design and electromagnetic diffraction theory. Since 1994, he has been with Alcatel-Lucent Bell-Labs. His work mainly focused on optical interconnects, wireless base station/handset RF circuits and systems, photonic circuits and subsystem modeling, ultra wide band RF-photonic systems, and recently silicon photonics. Prior to joining Bell-Labs he was a research fellow at University of Arizona, working in the area of holographic optical interconnects. He has authored or co-authored 50 papers in international journals and conference presentations, one book chapter, and holds five industrial patents.

Mahmoud S. Rasras received the Ph.D. degree in physics from the Catholic University of Leuven, Belgium, in 2000. His research on Spectroscopic Photon Emission Microscopy for CMOS-based semiconductor device reliability evaluation and testing was carried out at the Interuniversity Micro Electronics Center (IMEC).

In March 2001, he joined the Integrated Photonics Research Department at Bell Labs in Murray Hill where he is designing components for next generation optical networks. He is currently working on CMOS-compatible silicon-based integrated photonics circuits toward the monolithic integration of electronics with advanced optical components. He is also involved in research on an all-optical logic technology, where logical functions are realized in a hybrid silica/InP platform. He authored and coauthored more than 45 journal and conference papers. He also holds 7 US issued patents.

Dr. Rasras received Roger A. Haken Best Student Paper Award for his work on understanding thin CMOS gate oxide degradation at the 1999 IEDM conference.

Douglas M. Gill received the B.S. degree in physics from Buffalo State University College, NY, in 1987. He received the M.S. and Ph.D. degrees in the materials science program from the University of Wisconsin-Madison in 1994.

He held a Research Associate position at Northwestern University, and is currently a Member of Technical Staff at Bell Labs of Alcatel-Lucent at Murray Hill, NJ. His research interests include high-speed electro-optic transmitter design, the development of novel CMOS compatible electro-optic and thermo-optic photonic components, and the application of advanced transmission formats for cost effective data transmission.

Dr. Gill received the Newport research award for his graduate research. He holds over 20 patents, and 50 referred journal articles and conference proceedings.

Sanjay S. Patel received the B. Tech. Degree in chemical engineering from the Indian Institute of Technology Kanpur, Kanpur, India, and the Ph.D. degree in chemical engineering and material science degree from the University of Minnesota, Minneapolis.

He is currently the Lead Strategist in the CTO Office of the Wireline Division, Alcatel-Lucent, Murray Hill, NJ, where he is engaged in passive optical network technologies, and is the Asia-Pacific Product Line Manager for the Fiber-to-the-Home Product Group and a member of Bell Laboratories, where he was a Technical Manager for integrated photonic research and led a team that developed new ways of monolithically integrating optical components onto high-volume silicon IC platforms, and was involved in the modeling of absorption of cell-phone radiation in humans, self-assembly of 3-D photonic bandgap structures, sol-gel manufacturing of optical fibers, modeling of polymer dynamics, and designing new materials for holographic storage.

Young-Kai Chen (S'78–M'86–SM'94–F'98) received the B.S.E.E degree from the National Chiao Tung University, Hsinchu, Taiwan, and the M.S.E.E. degree from Syracuse University, Syracuse, NY, and the Ph.D. degree from Cornell University, Ithaca, NY, 1988.

From 1980 to 1985, he was a member of the Technical Staff in the Electronics Laboratory, General Electric Company, Syracuse, where he was responsible for the design of silicon and GaAs monolithic microwave ICs for phase array applications. Since Feburary 1988, he has been with Bell-Laboratories, Murray Hill, NJ, where he was a member of Technical staff, where he has been a Director of High Speed Electronics and Optoelectronics Research since 1994. He was an Adjunct Associated Professor at Columbia University. His current research interests include high-speed semiconductor devices, and circuits for wireless and optical fiber communications. He has authored or coauthored more than 100 technical papers and holds 15 patents in the field of high-frequency electronics devices, circuits, and semiconductor lasers.

Dr. Chen is a Fellow of Bell-Laboratories and an elected member of the National Academy of Engineering. He was the recipient of 2002 IEEE David Sarnoff Award.

Alice E. White (M'09) received the B.A. degree in physics from Middlebury College, Middleburry, VT, and the M.A. and Ph.D. degrees in physics from Harvard University, Cambridge, MA.

She is currently the Vice President of Bell-Laboratories, Alcatel-Lucent, Murray Hill, NJ. She has a broad technical background in experimental solid-state physics and optics, including fabrication and implementation of optical fiber devices and integrated optical components for optical networks, semiconductor processing and devices, ion-beam interactions with solids, and low temperature and vacuum techniques. She has authored or coauthored more than 125 papers.

Dr. White is an active member of American Physical Society (APS) and the Optical Society of America. She was a Fellow of the APS in 1995. She was the Councilor-at-Large for the APS in 1993 and was one of the founding members of the Forum on Industrial and applied Physics of the APS. She received the 1991 Maria Goeppert-Mayer Award from the APS. More recently, she received the prestigious Bell Laboratories Fellow Award.

Andrew Pomerene, photograph and biography unavailable at time of publication.

Daniel Carothers, photograph and biography unavailable at time of publication.

James Beattie, photograph and biography unavailable at time of publication.

Mark Beals, photograph and biography unavailable at time of publication.

Jurgen Michel, photograph and biography unavailable at time of publication.

Lionel C. Kimerling, photograph and biography unavailable at time of publication.